RSC Advances

PAPER

View Article Online
View Journal | View Issue

Check for updates

Cite this: *RSC Adv.*, 2020, **10**, 15199

Ultrafast broadband nonlinear optical properties and excited-state dynamics of two bis-chalcone derivatives

Lei Shen,[a] Zhongguo Li,*[b] Xingzhi Wu,[c] Wenfa Zhou,[d] Junyi Yang*[a] and Yinglin Song*[ae]

The development of organic nonlinear optical (NLO) chromophores is vital for various fields such as two-photon biomedical imaging, optical limiting, *etc.* In this work, two bis-chalcone molecules 1,4-bis[3-(2,4-dimethoxyphenyl)-2-acryloyl]benzene (**C1**) and 4,4′-bis[3-(2,4-bimethoxy phenyl)-2-acryloyl]biphenyl (**C2**) were synthesized and characterized. The excited-state dynamics of these two chromophores were studied using femtosecond transient absorption (TA) measurements. And their broadband nonlinear absorption properties and optical limiting (OL) response were investigated by femtosecond open-aperture Z-scan and intensity-dependent transmittance measurements in the wavelength range from 515 nm to 800 nm, respectively. The TA results demonstrate that **C2** has strong excited-state absorption behavior and longer lifetime. In addition, the nonlinear absorption response of **C2** was found to be superior to that of **C1** in the visible range after 500 nm, which is attributed to a two-photon-absorption induced excited-state absorption mechanism. These results indicate that the nonlinear optical response and excited-state dynamics in bis-chalcone compounds could be enhanced *via* intramolecular charge-transfer.

Received 19th February 2020
Accepted 31st March 2020

DOI: 10.1039/d0ra01592j

rsc.li/rsc-advances

Open Access Article. Published on 17 April 2020. Downloaded on 2/12/2026 11:22:30 PM.
This article is licensed under a Creative Commons Attribution-NonCommercial 3.0 Unported Licence.

1. Introduction

Organic nonlinear optical (NLO) materials have attracted considerable attention in recent years due to their intriguing properties, such as structural flexibility, large π-conjugated systems, and biocompatibility, and are highly promising for applications in all-optical switching, optical limiting, bio-imaging, and so on.[1–5] It is well known that the NLO response of conjugated organic materials is closely related to the structure of the molecule, such as the size of the π-conjugated system and the introduction of electron donor and electron acceptor.[6–10] Hence, designing novel organic chromophores exhibiting superior NLO response is of great scientific and technological interest not only for shedding light on the nonlinear light–matter interaction but also for the development of novel photonic devices. Chalcone derivatives are a kind of π-conjugated molecules and have been widely investigated in biology and medical science.[11–14] In recent years, they have received much interest due to the high tendency to crystallize and notable second and third-order NLO responses.[15–17] Dharmaprakash *et al.* have synthesized numerous chalcone derivatives and mainly investigated the crystalline perfection, third-order NLO and OL properties.[18–22] Despite these effects, however, the NLO mechanism and excited-state dynamics of these chalcone chromophores remains elusive.[23] Gu *et al.* studied the NLO properties of chalcone derivatives and proposed that their NLO response could be attributed to the multi-photon absorption induced excited-state absorption mechanism (MPA induced ESA).[24–26] Bis-chalcone is a derivative of chalcone, which has a larger π-conjugated electron system in its molecule skeleton. Although advances have been made towards investigating the NLO properties of bis-chalcones derivatives, however, the novel bis-chalcones compound with broadband ultrafast NLO response remains elusive.[27–30]

Albota *et al.* reported that symmetric charge transfer from the end of a conjugated system to the middle or *vice versa* can lead to large two-photon cross-section.[31] Following this idea, two bis-chalcone derivatives **C1** (ref. 32) and **C2** (Scheme 1) were synthesized and characterized. Their ultrafast excited-state dynamics were investigated using femtosecond TA measurements. And their broadband NLO responses and mechanism were also studied *via* femtosecond Z-scan technique in the visible regime. Our results show that the introduction of benzene ring to the bis-chalcone compound has a substantial impact on the excited-state absorption spectra and dynamics of

[a]*School of Physical Science and Technology, Soochow University, Suzhou 215006, China. E-mail: 15962196650@163.com*

[b]*School of Electronic and Information Engineering, Changshu Institute of Technology, Changshu 215500, China. E-mail: claes.lee@gmail.com*

[c]*Jiangsu Key Laboratory of Micro and Nano Heat Fluid Flow Technology and Energy Application, School of Mathematics and Physics, Suzhou University of Science and Technology, Suzhou 215009, China*

[d]*School of Optoelectronic Science and Engineering, Soochow University, Suzhou 215006, China*

[e]*Department of Physics, Harbin Institute of Technology, Harbin 150001, China. E-mail: ylsong@hit.edu.cn*

Open Access Article. Published on 17 April 2020. Downloaded on 2/12/2026 11:22:30 PM.
This article is licensed under a Creative Commons Attribution-NonCommercial 3.0 Unported Licence.

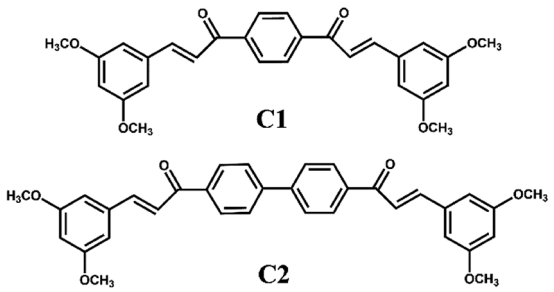

Scheme 1 Molecular structure of **C1** and **C2**.

these chromophores. And the nonlinear absorption properties of **C2** is greatly enhanced compared to that of **C1**, indicating **C2** compound is a promising OL material.

2. Experimental section and theoretical calculation

2.1 Synthesis and characterization of C1 and C2

Synthesis of 1,4-bis[3-(2,4-dimethoxyphenyl)-2-acryloyl] benzene (C1). A mixture of 1,4-diacetylbenzene (350 mg, 2 mmol) and 2,4-dimethoxy benzaldehyde (720 mg, 4 mmol) were placed in a 250 cm^3, three-necked, round-bottom flask. Methanol (45 ml) was added to it, and the flask was heated until the mixture dissolved completely. Sodium hydroxide (600 mg) as the catalyst was added to the reaction system. The reaction time was about 8 h (until the color of reaction liquid changes from light yellow to yellow). The reaction mixture was extracted and filtered, and the filter cake was washed with water and anhydrous ethanol twice, respectively. After recrystallized by anhydrous ethanol, 0.81 g of yellow powder solid crude product was obtained. The compound **C1** (350 mg, 35%) was obtained by column chromatography separation. ^{1}H NMR δ/ppm (600 MHz, DMSO-d): 8.225 (s, 4H), 8.053–8.027 (d, 2H, $J = 15.6$ Hz), 7.971–7.957 (d, 2H, $J = 8.4$ Hz), 7.816–7.790 (d, 2H, $J = 15.6$ Hz), 6.666–6.649 (d, 4H, $J = 11.2$ Hz), 3.920 (s, 6H), 3.859 (s, 6H). ^{13}C NMR δ/ppm (150 MHz, DMSO-d): 189.35, 163.86, 160.63, 141.46, 140.00, 130.84, 129.05, 119.51, 116.26, 106.96, 98.78, 56.37, 56.07. LC-MS (ESI, m/z): 459.15 $[M + H]^+$. Calcd. for $C_{28}H_{27}O_6$: 459.18.

Synthesis of 4,4′-bis[3-(2,4-bimethoxy phenyl)-2-acryloyl] biphenyl (C2). A mixture of 4,4-diacetyl biphenyl (476 mg, 2 mmol) and 2,4-dimethoxy benzaldehyde (730.4 mg, 4.4 mmol) were placed in a 250 cm^3, three-necked, round-bottom flask. Absolute ethyl alcohol (90 ml) was added to it, and the flask was heated until the mixture dissolved completely. Sodium hydroxide (10%, 5 ml) as the catalyst was added to the reaction system. The reaction time was about 40 h. The reaction mixture was extracted and filtered, and the filter cake was washed with anhydrous ethanol. The compound **C2** (100 mg, 10%) was obtained by column chromatography separation. ^{1}H NMR δ/ppm (600 MHz, $CDCl_3$): 8.146–8.132 (d, 4H, $J = 8.4$ Hz), 8.105 (s, 2H), 7.799–7.785 (d, 4H, $J = 8.4$ Hz), 7.630–7.616 (d, 2H, $J = 8.4$ Hz), 7.616–7.604 (d, 2H, $J = 7.2$ Hz), 6.585–6.571 (t, 2H, $J = 4.2$ Hz), 6.567–6.512 (t, 2H, $J = 16.5$ Hz), 3.941 (s, 6H), 3.890 (s, 6H). ^{13}C NMR δ/ppm (150 MHz, $CDCl_3$): 190.57, 163.14, 160.50, 143.83, 140.76, 138.25, 131.09, 129.15, 127.35, 120.31, 117.14, 105.46, 98.49, 55.60, 55.54. LC-MS (ESI, m/z): 535.20 $[M + H]^+$. Calcd. for $C_{34}H_{30}O_6$: 535.21 (Scheme 2).

2.2 Quantum chemical calculations

In order to investigate the influence of molecular structure on the NLO properties of the two compounds, quantum chemical calculation of density functional theory (DFT) was performed using the Gaussian 09 program package to obtain frontier molecular orbital distributions. The structures of the compounds was optimized by the B3LYP/6-31G (D, P) model. The energy and electron cloud distribution of frontier molecular orbitals were calculated. To further analyse the electron transition, the time-dependent density functional theory (TD-DFT)[33] was performed using the CAM-B3LYP functional[34] and the b3lyp/6-311g(d) basis set. The type of electron transition can be characterized through hole–electron analysis which was performed using Multiwfn 3.7 program.[35] The data of the density isosurface were extracted from Multiwfn and visualized by the VMD program.[36]

2.3 Transient optical nonlinearity

Ultrafast TA measurements were performed in ambient atmosphere at room temperature. A detailed description of the experimental system is reported elsewhere.[27] In brief, the 400 nm pump pulse was generated by an optical parametric amplifier (OPA, ORPHEUS, light conversion) pumped by a mode-locked Yb: KGW based fiber laser (PHAROS, light conversion). The laser pulse duration and repetition rate were 190 fs and 6 kHz, respectively. The probe light was the white-light supercontinuum generated using sapphire crystal. The instrument response function (IRF) was estimated to be around 250 fs. In order to minimize the high-order dynamics, the pump energy was kept below 12 mW.

2.4 Nonlinear absorption experiments

The nonlinear absorption and optical limiting properties of **C1** and **C2** were measured by open-aperture Z-scan[37] and intensity-dependent transmittance measurement with the same femtosecond laser source in fs TA experiments. The pulse duration and laser repetition rate were 190 fs and 20 Hz, respectively. The sample compounds were diluted in DMSO solvent with a concentration of 4×10^{-3} M and contained in 2 mm quartz cells. The neat DMSO solvent was also measured under the same experimental condition and the solvent's NLO response was removed in the data analysis.

3. Results and discussions

3.1 UV-vis absorption and florescence spectra

The UV-vis absorption spectra and fluorescence spectra of bis-chalcone derivatives **C1** and **C2** are shown in Fig. 1. The measurements were carried out in dilute DMSO (2×10^{-5} M) at room temperature. The results demonstrate that the change in absorption peak of **C1** and **C2** is rather small (387 nm *vs.* 378

 This journal is © The Royal Society of Chemistry 2020

Open Access Article. Published on 17 April 2020. Downloaded on 2/12/2026 11:22:30 PM.
This article is licensed under a Creative Commons Attribution-NonCommercial 3.0 Unported Licence.

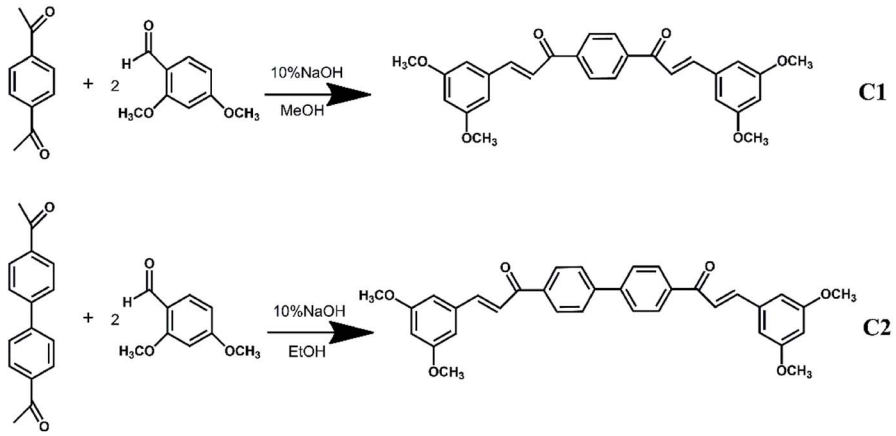

Scheme 2 Synthetic route of target compounds C1 and C2.

nm), but their emission maximum have dramatic changes (536 nm and 490 nm). The fluorescence spectrum band of **C2** showed blue-shifted compared to that of **C1**, which indicate the strong intramolecular charge-transfer character in **C2**.[38] This charge-transfer character can also be supported by the DFT calculation results in Fig. 2.

As can be seen in Fig. 2, the electron moiety transition is corresponded with the maximum absorption peak on the absorption spectra from HOMO to LUMO ability. The HOMO–LUMO energy gap of **C1** and **C2** are 3.40 eV and 3.46 eV, respectively. And these results corresponded to the UV-vis absorption.

Fig. 3 shows the hole and electron distributions of the two compounds. Red and grey isosurfaces denote where electrons increase (electron) and where electrons decrease (hole), respectively. The transition energies (between S0 and S1) of the two compounds were calculated to be 2.956 and 3.034 eV, respectively. The results of Fig. 3 clearly show that **C2** has strong intramolecular charge-transfer. And compared with **C1**, **C2** has more π-electrons.

3.2 Transient absorption spectrum

Fig. 4(a) and (b) show the TA spectra of **C1** and **C2** in DMSO solution, respectively. The evolution associated difference spectra (EADS) for **C1** and **C2** are plotted in Fig. 4(c) and (d), respectively. In Fig. 4(c), the TA spectrum at a delay of 0.55 picosecond (ps) after 400 nm laser excitation is characterized by an excited state absorption (ESA) band with peak before 460 nm and a stimulated emission (SE) peak at about 540 nm. The transient spectrum evolves in 20 ps, exhibiting a dynamic red shift of the SE band maximum to 610 nm which may attribute to the vibrational relaxation of S1. With further time delay, the ESA band and SE band decays up to about 400 ps. The TA spectral evolution of **C1** suggests three distinct relaxation processes which occur in 0–0.25 ps, 0.25–20 ps, 20–350 ps, 350 ps–ns time scales. Through global analysis[39] (see Fig. 5(a)), we obtain four dynamic processes and the lifetimes are about 0.25 ps, 4.9 ps, 142.8 ps and 2.9 ns, respectively. The first content is unable to be distinguished as the time resolution of our experiment is 0.25 ps. So we assign the ultrafast process of 0.25 ps to the internal conversion in the first singlet state (S1). The next component with a 4.9 ps lifetime corresponds to the vibrational relaxation of S1. The last two times are then assigned to the inter-system crossing (ISC) process between singlet and triplet state (142.8 ps) and lifetime of the triplet state (2.9 ns).[40,41]

As shown in Fig. 4(d), the TA spectra of **C2** underwent dramatic changes compared to the TA spectra of **C1**. Following 400 nm laser excitation, the TA spectrum at 0.2 ps is characterized by an excited state absorption (ESA) band with peak at around 540 nm. The valley at about 485 nm attributes to the competition between ESA and the effect of fluorescence. The ESA peak at 540 nm exhibits a red shift with a decrease in

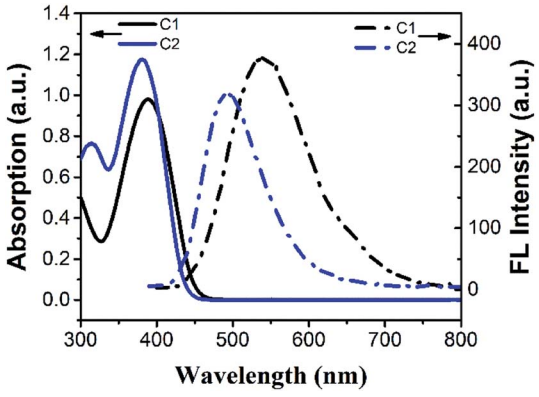

Fig. 1 UV-vis absorption (solid lines) and emission spectrum (dashed lines) of C1 (black) and C2 (blue).

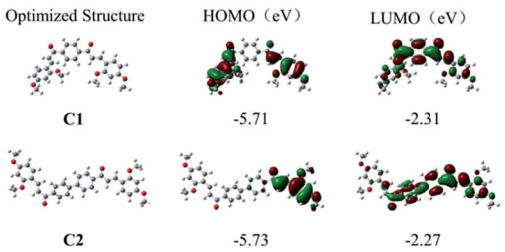

Fig. 2 Frontier molecular orbital distributions of C1 and C2.

Open Access Article. Published on 17 April 2020. Downloaded on 2/12/2026 11:22:30 PM.
This article is licensed under a Creative Commons Attribution-NonCommercial 3.0 Unported Licence.

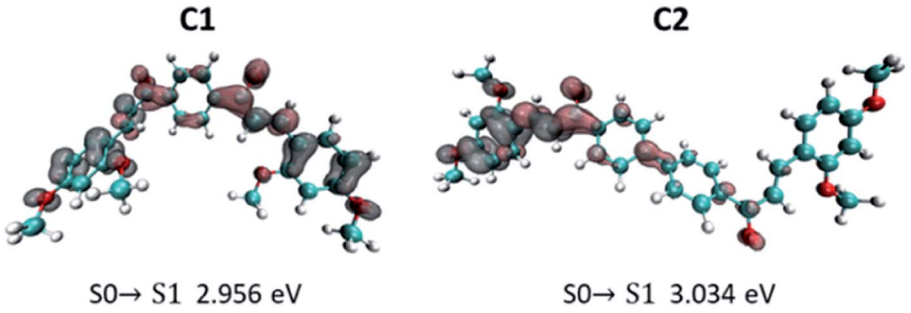

Fig. 3 Hole and electron distributions of **C1** and **C2**.

intensity within 1.4 ps. With further time delay, a new ESA band grows in the 450–550 nm region. After 12 ps, on further delay, ESA decay in the 1100 ps time scale. And then follows a much longer ESA decay in the time scale of ns. Through global analysis (see Fig. 5(b)), we obtain four similar dynamic processes with **C1** and the lifetimes are about 0.25 ps, 7.5 ps, 144.8 ps and 7 ns, respectively. It can be easily seen in Fig. 5, unlike **C1**, with the improvement of the molecule, the relaxation process of excited state has been changed and the lifetime becomes longer (from 2.9 ns to 7 ns). Furthermore, there's no SE in the TA spectrum of **C2**. And the intensity of ESA of **C2** is stronger than that of **C1** in the visible range after 500 nm which means the nonlinear optical properties of **C2** can be improved because of more π-electrons in **C2**.[42–44] The TA spectra indicate that the excited-state relaxation processes change dramatically with the molecule structure change from **C1** to **C2**, which could be related to the stronger intramolecular charge-transfer character in **C2**.

3.3 Femtoseconds Z-scan experiment

To investigate the nonlinear optical response of these two compounds, open-aperture Z-scan measurements were carried out at different laser intensity in wavelength range of 515–800 nm. The concentration of **C1** and **C2** were about 5.2 × 10^{-3} mol L^{-1}. The contribution of solvent's NLO response was subtracted in the data fitting. The experimental results show that **C2** has larger reverse saturation absorption (RSA) than **C1** in the whole wavelength range. Due to the fs laser pulses used in the Z-scan measurements, the main RSA mechanism should be intrinsic multi-photon absorption. To further analyze the mechanism of the observed optical nonlinearities, all Z-scan measurements were carried out under different laser intensity. And the variation of nonlinear absorption coefficient with different laser irradiance at 600 nm was plotted in Fig. 6(c).

By fitting to the Z-scan theory,[37] the effective nonlinear absorption β_{eff} at different intensities were obtained. From Fig. 6(c), the extracted β_{eff} of **C1** is observed to remain substantially unchanged, indicating that 2 PA may be the only mechanism under this wavelength. In contrast, the β_{eff} of **C2** is nearly a proportionally increasing function of the intensity I_0, which means there was higher-order nonlinear absorption. Due to the laser wavelength is far away from the potential 3PA window (>1100 nm), the higher-order nonlinear absorption can be attributed to the 2PA-induced ESA.[45–47] Therefore, the Z-scan results in Fig. 6 agree well with the fs TA measurements of the two compounds. According to the 2PA-induced ESA theory, the nonlinear absorption coefficient can be expressed as $\alpha = \alpha_0 + \beta I + \gamma I^2$, where α_0, β and γ represent the linear absorption, TPA,

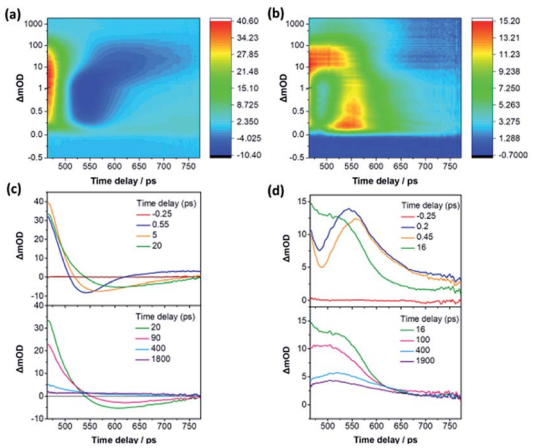

Fig. 4 TA spectra of **C1** (a) and **C2** (b) diluted in DMSO at excitation wavelength of 400 nm. (c and d) Plots of the TA spectra at various time delays of **C1** and **C2**, respectively.

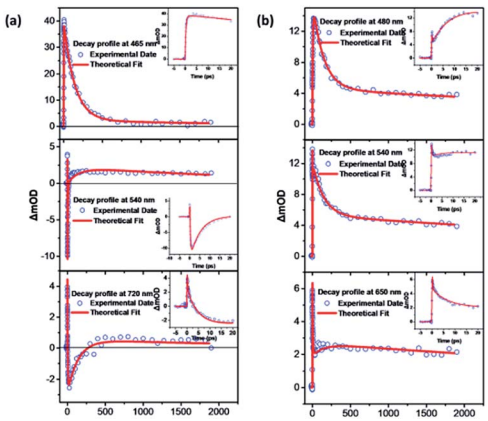

Fig. 5 (a and b) Temporal dynamics of **C1** and **C2** in DMSO following femtosecond laser excitation at 400 nm, respectively. Inset figures show early stage dynamics of the same (within the first 20 ps). Circles are experimental data, and solid lines represent theoretical fitting.

This journal is © The Royal Society of Chemistry 2020

Open Access Article. Published on 17 April 2020. Downloaded on 2/12/2026 11:22:30 PM.
This article is licensed under a Creative Commons Attribution-NonCommercial 3.0 Unported Licence.

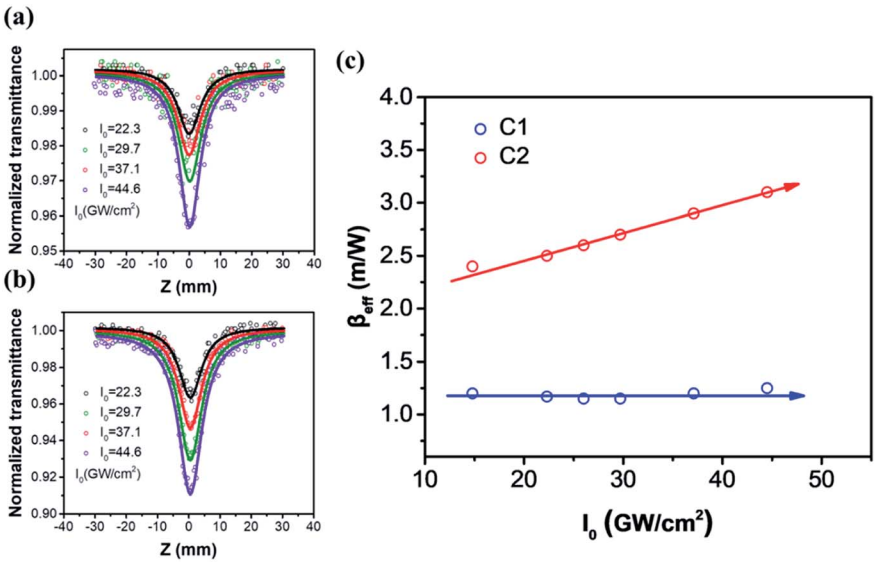

Fig. 6 (a and b) Open-aperture Z-scan curves of **C1** and **C2** at 600 nm under 190 fs excitation, respectively. Circles are experimental data, and solid lines represent theoretical fitting. (c) Example of the intensity dependence of the nonlinear absorption coefficient for **C1** and **C2**.

and the effective fifth-order nonlinear absorption coefficients, respectively. And the TPA cross section σ_{TPA} can be achieved by the equation $\sigma_{TPA} = h\omega\beta/N$. Both β and γ can be determined by theoretical fitting the Z-scan curves in different laser intensity. All NLO parameters of the two compounds are summarized in Table 1. The experimental error was less than 10%.

From Table 1, it is shown that both compounds exhibit TPA induced ESA in the whole wavelength window from 515 nm to 800 nm, except for **C1** compound in around 600 nm. The results also demonstrate that the two-photon absorption coefficients β and TPA cross section σ_{TPA} of **C2** are substantially larger than **C1**, which indicate that **C2** has promising nonlinear absorption response in the visible regime.

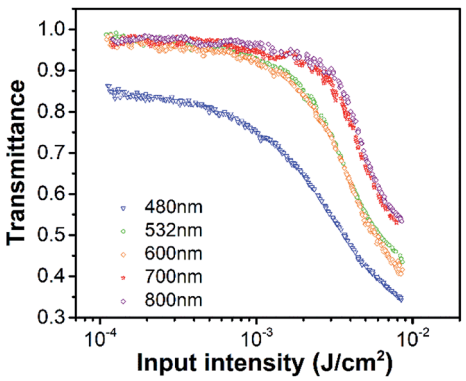

Fig. 7 Ultrafast OL of **C2** as a function of the input fluence at 480 nm, 532 nm, 600 nm, 700 nm and 800 nm with 190 fs excitation.

3.4 Optical limiting behaviour

From previous analysis, **C2** compound has strong ICT and exhibits favorable TPA and ESA,[45,46] which means it may have strong optical limiting response in the visible wavelength regime. Fig. 7 shows the variations of the transmittance of **C2** diluted in DMSO as a function of the input laser fluence at 480, 532, 600, 700 and 800 nm. The sample solution was contained in a 10 mm thick cuvette. Fig. 7 shows that the **C2** shows high linear transmittance at all wavelengths (0.85–0.98). And the transmittance of **C2** solution decreases with increasing input

Table 1 The experimental results of TPA and TPA induced ESA at different wavelength from open-aperture Z-scan measurements

Wavelength (nm)	C1			C2		
	β (10^{-2} cm GW^{-1})	σ_{TPA} (GM)	γ (10^{-4} cm^3 GW^{-2})	β (10^{-2} cm GW^{-1})	σ_{TPA} (GM)	γ (10^{-4} cm^3 GW^{-2})
515	0.50	80.2	2.0	0.63	101.0	2.9
532	0.95	139.7	2.5	1.1	170.7	2.7
580	0.9	128.2	0.75	1.99	283.4	2
600	1.19	163.8	0	1.99	274.0	2.4
650	0.4	50.8	0.2	0.7	88.9	0.25
700	0.66	77.9	0.15	0.95	112.1	0.2
800	0.6	67.1	0.17	0.9	92.9	0.25

Open Access Article. Published on 17 April 2020. Downloaded on 2/12/2026 11:22:30 PM.
This article is licensed under a Creative Commons Attribution-NonCommercial 3.0 Unported Licence.

Table 2 Summary of the OL parameters of **C2** and other materials

Sample	λ/pulse	Wavelength (nm)	T (%)	Threshold (10^{-3} J cm^{-2})	Ref.
C2/DMSO	190 fs	480	85	4.9	This work
		532	98	6.5	
		600	98	5.9	
		700	98	10.3	
		800	98	12.9	
Pyrene-based molecules/DMSO	190 fs	515–900	>91	≈19	45
Hydrazone derivatives/DMF	190 fs	515–800	72–98	2.75–10.6	46
Fluorescent stilbene dye/$CHCl_3$	100 fs	800	—	30 100	38
Silver nanoparticle-embedded polymer film	110 fs	800	94	154	48
a-Se doped silica	100 fs	800	85	450	49
QD	8 ns	532, 1064	—	>720	50
Grapheme/water	8 ns	532, 1064	70	>500	51
CNT/water	3–80 ns	430–1064	—	70–947	52
CNT/chloroform	3–80 ns	430–1064	—	13–740	52

irradiance. The properties of OL material is shown as the OL threshold, which is the laser fluence when the transmittance of the sample decreases to 50% of the original value. The OL threshold of **C2** and other organic materials reported in recent literatures are summarized in Table 2.[38,45,46,48–52] The results in Table 2 show that the **C2** compound has strong OL response compared to other organic compounds and inorganic nanomaterials, which means it's a promising ultrafast broadband optical limiter. Based on the fs TA and Z-scan measurements above, the OL response of **C2** can be attributed to the TPA induced ESA mechanism.

4. Conclusions

In summary, two bis-chalcone derivatives **C1** and **C2** were successfully synthesized and characterized by UV-vis, fluorescent spectra and DFT and TD-DFT calculation. And their nonlinear optical response and excited-state dynamics were characterized using broadband femtosecond Z-scan measurement and transient absorption measurements, respectively. The fs TA spectra demonstrate that **C2** has strong excited-state absorption behaviour and longer excited-state lifetime compared to **C1**. Remarkably, the Z-scan measurements show that the nonlinear absorption response of **C2** is stronger than **C1** in range of 515 nm to 800 nm under the excitation of fs laser pulse, which is attributed to the 2PA-induced ESA mechanism. These results indicate that the nonlinear optical response and excited-state dynamics in bis-chalcone chromophore can be fine-tuned by intramolecular charge-transfer process. Our results clearly demonstrate the bis-chalcone derivatives **C2** with excellent nonlinear absorption and longer lifetime can be promising candidate for future applications in optical limiting, bio-imaging, *etc.*

Conflicts of interest

There are no conflicts to declare.

Acknowledgements

The authors gratefully acknowledge the support of the NSAF (Grant No. U1630103), Special Fund from State Key Laboratory of Intense Pulsed Radiation Simulation and Effect (Grant No. SKLIPR1715) and National Natural Science Foundation of China (Grant No. 11704048, 11804244).

References

1 Y. Song, Y. Chen, X. Jiang, W. Liang, K. Wang, Z. Liang, Y. Ge, F. Zhang, L. Wu and J. Zheng, *Adv. Opt. Mater.*, 2018, **6**, 1701287.
2 X. Li, R. Liu, H. Xie, Y. Zhang, B. Lyu, P. Wang, J. Wang, Q. Fan, Y. Ma and S. Tao, *Opt. Express*, 2017, **25**, 18346–18354.
3 I. I. Smolyaninov, *J. Opt. Soc. Am. B*, 2019, **36**, 1629–1636.
4 S. J. Varma, J. Kumar, Y. Liu, K. Layne, J. Wu, C. Liang, Y. Nakanishi, A. Aliyan, W. Yang and P. M. Ajayan, *Adv. Opt. Mater.*, 2017, **5**, 1700713.
5 Y. Tamgadge, A. Sunatkari, S. Talwatkar, V. Pahurkar and G. Muley, *Opt. Mater.*, 2016, **51**, 175–184.
6 B. Jędrzejewska, P. Krawczyk, M. Pietrzak, M. Gordel, K. Matczyszyn, M. Samoć and P. Cysewski, *Dyes Pigm.*, 2013, **99**, 673–685.
7 M. Tasior, K. Hassanein, L. M. Mazur, I. Sakellari, D. Gray, M. Farsari, M. Samoć, F. Santoro, B. Ventura and D. T. Gryko, *Phys. Chem. Chem. Phys.*, 2018, **20**, 22260–22271.
8 L. M. Mazur, T. Roland, S. Leroy-Lhez, V. Sol, M. Samoc, I. D. Samuel and K. Matczyszyn, *J. Phys. Chem. B*, 2019, **123**, 4271–4277.
9 J. Jia, J. Zhang, C. Zhou, M. Zheng, D. Feng, G. Liang and Y. She, *Dyes Pigm.*, 2019, **166**, 314–322.
10 M. de Torres, S. Semin, I. Razdolski, J. Xu, J. A. Elemans, T. Rasing, A. E. Rowan and R. J. Nolte, *Chem. Commun.*, 2015, **51**, 2855–2858.
11 Z. Rozmer and P. Perjési, *Phytochem. Rev.*, 2016, **15**, 87–120.

 This journal is © The Royal Society of Chemistry 2020

Open Access Article. Published on 17 April 2020. Downloaded on 2/12/2026 11:22:30 PM.
This article is licensed under a Creative Commons Attribution-NonCommercial 3.0 Unported Licence.

12 P. M. Sivakumar, S. Cometa, M. Alderighi, V. Prabhawathi, M. Doble and F. Chiellini, *Carbohydr. Polym.*, 2012, **87**, 353–360.
13 A. Foroumadi, S. Emami, M. Sorkhi, M. Nakhjiri, Z. Nazarian, S. Heydari, S. K. Ardestani, F. Poorrajab and A. Shafiee, *Chem. Biol. Drug Des.*, 2010, **75**, 590–596.
14 S. Chowdhary, P. Bhoj, S. Bahekar, N. Togre, K. Goswami and H. Chandak, *J. Mahatma Gandhi Inst. Med. Sci.*, 2017, **22**, 128.
15 S. R. Maidur, P. S. Patil, S. V. Rao, M. Shkir and S. Dharmaprakash, *Opt. Laser Technol.*, 2017, **97**, 219–228.
16 P. Patil, S. R. Maidur, S. V. Rao and S. Dharmaprakash, *Opt. Laser Technol.*, 2016, **81**, 70–76.
17 P. S. Patil, S. R. Maidur, M. Shkir, S. AlFaify, V. Ganesh, K. N. Krishnakanth and S. V. Rao, *J. Appl. Crystallogr.*, 2018, **51**, 1035–1042.
18 P. Patil, M. Bannur, D. Badigannavar and S. Dharmaprakash, *Opt. Laser Technol.*, 2014, **55**, 37–41.
19 T. C. S. Shetty, S. Raghavendra, C. C. Kumar, S. Naveen, S. R. Maidur, P. S. Patil, S. Chandraju, G. Ananthnag and S. Dharmaprakash, *Opt. Mater.*, 2018, **86**, 138–147.
20 T. C. S. Shetty, S. Raghavendra, C. C. Kumar and S. Dharmaprakash, *Appl. Phys. B: Lasers Opt.*, 2016, **122**, 205.
21 P. Patil, S. Dharmaprakash, H.-K. Fun and M. Karthikeyan, *J. Cryst. Growth*, 2006, **297**, 111–116.
22 P. Patil, S. Dharmaprakash, K. Ramakrishna, H.-K. Fun, R. S. S. Kumar and D. N. Rao, *J. Cryst. Growth*, 2007, **303**, 520–524.
23 H. Song, Z. Kuang, X. Wang, Y. Guo, Q. Guo, H. Zhang and A. Xia, *J. Phys. Chem. C*, 2018, **122**, 15108–15117.
24 B. Gu, W. Ji, X.-Q. Huang, P. Patil and S. Dharmaprakash, *Opt. Express*, 2009, **17**, 1126–1135.
25 B. Gu, W. Ji, P. Patil, S. Dharmaprakash and H.-T. Wang, *Appl. Phys. Lett.*, 2008, **92**, 091118.
26 B. Gu, W. Ji, H.-Z. Yang and H.-T. Wang, *Appl. Phys. Lett.*, 2010, **96**, 081104.
27 Y. Yang, X. Wu, J. Jia, L. Shen, W. Zhou, J. Yang and Y. Song, *Opt. Laser Technol.*, 2020, **123**, 105903.
28 P. Poornesh, K. Ravi, G. Umesh, P. K. Hegde, M. Manjunatha, K. Manjunatha and A. Adhikari, *Opt. Commun.*, 2010, **283**, 1519–1527.
29 A. M. Asiri and S. A. Khan, *Mater. Lett.*, 2011, **65**, 1749–1752.
30 M. S. Kiran, B. Anand, S. S. S. Sai and G. N. Rao, *J. Photochem. Photobiol., A*, 2014, **290**, 38–42.
31 M. Albota, D. Beljonne, J.-L. Brédas, J. E. Ehrlich, J.-Y. Fu, A. A. Heikal, S. E. Hess, T. Kogej, M. D. Levin and S. R. Marder, *Science*, 1998, **281**, 1653–1656.
32 S. Tsukerman, V. Maslennikova, V. Nikitchenko and V. Lavrushin, *J. Appl. Spectrosc.*, 1970, **12**, 76–80.
33 F. Furche and R. Ahlrichs, *J. Chem. Phys.*, 2002, **117**, 7433–7447.
34 T. Yanai, D. P. Tew and N. C. Handy, *Chem. Phys. Lett.*, 2004, **393**, 51–57.
35 T. Lu and F. Chen, *J. Comput. Chem.*, 2012, **33**, 580–592.
36 W. Humphrey, A. Dalke and K. Schulten, *J. Mol. Graphics*, 1996, **14**, 33–38.
37 M. Sheik-Bahae, A. A. Said, T.-H. Wei, D. J. Hagan and E. W. Van Stryland, *IEEE J. Quantum Electron.*, 1990, **26**, 760–769.
38 T. He, S. Sreejith, Y. Gao, A. C. Grimsdale, Y. Zhao, X. Lin and H. Sun, *Appl. Phys. Lett.*, 2015, **106**, 111904.
39 I. H. Van Stokkum, D. S. Larsen and R. Van Grondelle, *Biochim. Biophys. Acta, Bioenerg.*, 2004, **1657**, 82–104.
40 R. M. van der Veen, A. Cannizzo, F. Van Mourik, A. Vlcek Jr and M. Chergui, *J. Am. Chem. Soc.*, 2011, **133**, 305–315.
41 Y. p. Wang, S. Zhang, S. m. Sun, K. Liu and B. Zhang, *Chin. J. Chem. Phys.*, 2013, **26**, 651–655.
42 F. Guo, W. Sun, D. Wang, L. Zhao, Z. Lu and Y. Nie, *Appl. Opt.*, 2001, **40**, 1386–1388.
43 J. Jia, X. Wu, Y. Fang, J. Yang, Y. Han, J. Xiao, X. Zhang, Y. Wang and Y. Song, *J. Phys. Chem. C*, 2020, **124**, 4701–4708.
44 T. C. Lin, Y. H. Lee, C. Y. Liu, B. R. Huang, M. Y. Tsai, Y. J. Huang, J. H. Lin, Y. K. Shen and C. Y. Wu, *Chem. - Eur. J.*, 2013, **19**, 749–760.
45 Z. Xiao, Y. Shi, R. Sun, J. Ge, Z. Li, Y. Fang, X. Wu, J. Yang, M. Zhao and Y. Song, *J. Mater. Chem. C*, 2016, **4**, 4647–4653.
46 J. Jia, X. Wu, Y. Fang, J. Yang, X. Guo, Q. Xu, Y. Han and Y. Song, *J. Phys. Chem. C*, 2018, **122**, 16234–16241.
47 R. Niu, Q. Chang, X. Wu, Y. Han, J. Jia, S. Chen and Y. Song, *Opt. Mater.*, 2018, **85**, 319–328.
48 S. Porel, N. Venkatram, D. N. Rao and T. Radhakrishnan, *J. Appl. Phys.*, 2007, **102**, 033107.
49 K. A. Mary, N. Unnikrishnan and R. Philip, *RSC Adv.*, 2015, **5**, 14034–14041.
50 Z. Xie, F. Wang and C. y. Liu, *Adv. Mater.*, 2012, **24**, 1716–1721.
51 M. Feng, H. Zhan and Y. Chen, *Appl. Phys. Lett.*, 2010, **96**, 033107.
52 L. Vivien, D. Riehl, P. Lancon, F. Hache and E. Anglaret, *Opt. Lett.*, 2001, **26**, 223–225.